Accuracy of Analog Fiber-optic Links for Inertial Confinement Fusion Diagnostics

Edward Kirk Miller, Gregory S. Macrum, Ian J. McKenna, Hans W. Herrmann, Joseph M. Mack, Carlton S. Young, Thomas J. Sedillo, Scott C. Evans, Colin J. Horsfield

***Abstract*—Interferometric fiber-optic links used in pulsed-power experiments are evaluated for accuracy in the presence of radiation fields which alter fiber transmission. Amplitude-modulated format (e.g., Mach-Zehnder) and phase-modulated formats are compared.**

***Index Terms*—Mach-Zehnder, Inertial-confinement Fusion, High-bandwidth Recording**

I. Introduction

HISTORICALLY, studies of radiation effects on optical fibers have focused on degradation and recovery of the fibers' transmission properties; such work is either in the context of survivability of fibers in catastrophic conditions or suitability of fibers installed for command and control systems within an experimental facility [1], [2]. In this work, we consider links used to transmit real-time diagnostic data, and we analyze the error introduced by radiation effects during the drive pulse. The result is increased uncertainties in key parameters required to unfold the sinusoidal transfer function. Two types of modulation are considered: amplitude modulation typical of a Mach-Zehnder (M-Z) modulator [3], and phase modulation, which offers more flexible demodulation options but relies on the spatiotemporal coherence of the light in the fiber. The M-Z link is shown schematically in Fig. 1, and the phase-modulated link is shown in Fig. 2.

We present data from two experimental environments: one with intense, controlled radiation fields to simulate conditions expected at the next generation of pulsed-power facilities, and the second with radiation effects below the noise level of the recording system. In the first case, we intentionally expose three types of single-mode fiber (SMF) to ionizing radiation and study the response by simultaneously monitoring phase and amplitude of the transmitted light. The phase and amplitude effects are evidently dominated by different physical phenomena, as their recovery dynamics are markedly different; both effects, though, show similar short-term behavior during exposure, integrating the dose at the dose levels studied, from 1 to 300 kRad, over the exposure times of 50 ps and 30 ns.

In the second case, we present data using a state-of-the-art fiber-optic link for single-shot transmission and recording, fielded at the OMEGA laser facility on high-yield fusion experiments. Gamma reaction history data are measured with a gas Cherenkov detector (GCD) [4], [5] and transmitted by M-Z link to a 12 GHz digitizer. Since radiation effects on the fibers are not above the noise floor, the error analysis for the unfolded data is dominated by the performance of the fast digitizer, the photoreceiver, and the laser.

Manuscript received July 19, 2007. This manuscript has been authored by National Security Technologies, LLC, under Contract No. DE-AC52-06NA25946 with the U.S. Department of Energy. The United States Government retains and the publisher, by accepting the article for publication, acknowledges that the United States Government retains a non-exclusive, paid-up, irrevocable, world-wide license to publish or reproduce the published form of this manuscript, or allow others to do so, for United States Government purposes.

E. K. Miller, G. S. Macrum, and I. J. McKenna are with National Security Technologies, LLC, Special Technologies Laboratory, Santa Barbara, CA 93111 USA. (E. K. Miller is corresponding author; phone: 805-681-2237; fax: 805-681-2280; e-mail: millerek@nv.doe.gov).

H. W. Herrmann, J. M. Mack, C. S. Young, T. J. Sedillo, and S. C. Evans are with Los Alamos National Laboratory, Los Alamos, NM 87545 USA.

C. J. Horsfield is with Atomic Weapons Establishment, Aldermaston, Berkshire RG7 4PR, United Kingdom.

II. Sources of Inaccuracy for Interferometric Fiber Links

A. Transfer Function

The accumulation of phase and the reduction in transmission during exposure must now be considered in the context of amplitude- and phase-modulated links for pulsed-radiation environments. The sinusoidal transfer function for an interferometric link modulated by input voltage V_{Input} can be written as:

$$V_{Measured} = \frac{V_{OutMax}}{2}\left[1+\sin\left(\frac{\pi V_{Input}}{V_{\pi}}-\varphi_0\right)\right], \quad (1)$$

where $V_{OutMax} = V_{Max} - V_{Min}$ with V_{Min} and V_{Max} defined as the estimated digitizer voltages corresponding to maximum and minimum transmission. $V_{Measured}$ is defined as the difference between $V_{Digitizer}$, the recorded photoreceiver voltage, and V_{π} is the modulator's half-wave voltage, typically 3–8 V for modern modulators.

Inversion of (1) gives the following expression for the instantaneous phase, $\varphi(t)$, related to the input voltage by $V_{Input} = V_{\pi} * \varphi / \pi$:

$$\varphi(t) = \sin^{-1}\left[2\frac{(V_{Meas}-V_{Min})}{(V_{Max}-V_{Min})}-1\right]+\varphi_0. \quad (2)$$

For amplitude-modulated links, like M-Z links, the uncertainty of the initial phase, φ_0, is a static value that is typically well-controlled in modern, bias-controlled systems; furthermore, the accuracy of φ_0 can typically be validated from the recorded data. The dynamic uncertainty, then, includes only the envelope, ($V_{Max} - V_{Min}$), and the digitizer record itself, $V_{Digitizer}$. This confounding of the amplitude-encoded signal with the radiation effects is problematic in cases where the modulator is operated in the "quasi-linear" mode, as the extrema are not recorded by the digitizer. In cases where the modulator is operated in "multi-fringe" mode, uncertainty in the envelope is greatly reduced, since discrete real-time values of the extrema are present in the digitizer record.

For phase-modulated links, the previous argument holds, in that the light amplitude is dynamically changing, and the envelope must be estimated. However, for links where demodulation of the phase-encoded data occurs outside of the radiation environment, the baseline, φ_0, will also generally be changing with time. Stated differently, phase shifts introduced by radiation incident on the fiber will become indistinguishable from the phase shift introduced by modulation in the electro-optic modulator.

With this formulation of the transfer function in terms of measured quantities, it is instructive to list explicitly the system components and environmental effects that create uncertainty in the unfold parameters.

--$V_{Digitizer}$ is impacted by noise in the laser, photoreceiver, and digitizer, as well as linearity in the receiver and digitizer.

--V_{Max} and V_{Min} are impacted by measurement of the pre-shot light level, bandwidth rolloff in the receiver and digitizer, and dynamic darkening of the fiber. In addition, V_{Min} is impacted by incomplete extinction of the light by the interferometer.

-- φ_0 is impacted by the accuracy of the bias control and measurement of the pre-shot light level. For phase-modulated links, φ_0 may be $\varphi_0(t)$ in the case where radiation is dynamically phase-shifting light in the fiber.

B. Estimating the Magnitude of Errors

Two approaches can be taken to estimating error bars on unfolded interferometer data. The first, and simplest, is to estimate uncertainties in the unfold parameters and perform Monte Carlo simulations of records, given those uncertainties. This approach works well for single records, and error bands (for example, at the 95% confidence level) can easily be generated from histograms of the simulated results. However, the magnitude of the error bar, then, no longer reflects correlation of errors, even though errors on neighboring points are correlated. Further analysis (e.g., least-squares spline-fitting to generate a composite curve from multiple records) [6] may not have adequate information from the errors generated by this Monte Carlo technique.

The second approach is to differentiate the transfer function with respect to the unfold parameters and use the uncertainties to generate a (generally non-diagonal) covariance matrix, which can then be used in a full least-squares fit [7].

In this paper, we present results from the first approach, taking $V_{Digitizer}$ as the dynamic parameter and V_{Min}, V_{Max}, and φ_0 as static parameters for Monte Carlo simulations. The details of the error magnitudes and the simulation are discussed in Section IV.

III. Magnitude of Radiation Effects on Transmission Fibers

An important design criterion for fiber links in a pulsed-radiation environment is the sensitivity of the transmission fibers to the radiation. Generally, both amplitude and phase may be affected by the pulsed radiation, so we have measured both simultaneously under two different but complementary conditions on three different commercially available fibers. For testing, we selected Corning SMF28e fiber, J-Fiber's radiation-hardened SMF, and Crystal Fibre solid-core photonic crystal fiber (PCF).

The first measurement is the sensitivity of the fibers using high doses (10–300 kRad) of 2 MeV electrons during the 30 ns pulse from a Febetron 705. The second measurement is the temporal response at much lower per-shot doses using the 50 ps pulses of 12 MeV electrons at the Idaho State University linear accelerator (LINAC).

The time scale for the high-dose experiment was chosen to reflect the relevant time scale for high-bandwidth fusion diagnostics. For such diagnostics, the transient response of the fiber is relevant to the accuracy of the recorded data only during (a) the initial radiation due to the drive pulse, (b) the radiation due to the fusion process, and (c) the transit time of the signal from the target chamber to the recorder. For a 30 m fiber run, the transit time dominates this expression, so for the purposes of this study, we concern ourselves with effects only during the initial 150 ns. Survivability of the link over many shots is a separate concern that is addressed by a variety of studies in the literature [1], [2], [9].

A. Experimental Setup

The source laser for all experiments was an NP Photonics *Scorpion* fiber laser at a wavelength of 1550.12 nm with a linewidth of approximately 5 kHz, giving it a coherence length much longer than the delay fiber used to demodulate the phase (30 m total). A length of SMF28e transmission fiber was used to deliver the light to the target area, where it was coupled to the fiber under test. Typical light power in the fiber was 10 mW; this light level is typical of the level required to fully drive modern, high-bandwidth photoreceivers after demodulating the phase using an interferometer based on a 3×3 coupler as we have done. Prior studies [1] have suggested that this constitutes "high-power" operation of fiber links, but the design of a system around commercially available components and digitizers drives the decision to use approximately 1 mW per photoreceiver, with the optical signal typically split between two or more receivers.

The phase of the transmitted light was demodulated using a

delay interferometer of approximately 150 ns delay in a Michelson configuration using a 3 × 3 directional coupler. The third output of the coupler was used to measure attenuation. The signals were recorded using 12 GHz photoreceivers and high-bandwidth real-time digitizers. The Febetron experiments used a 3 GHz digitizer in one-shot mode, and the LINAC experiments used a 12 GHz digitizer in averaging mode to achieve suitable signal-to-noise ratios.

For the Febetron experiments, the fiber under test was positioned approximately 30 cm from the face of the tube, with a 2.5 cm length exposed in an aperture created by lead bricks. Care was taken to ensure that no dose was delivered to portions of the fiber outside the experimental aperture. The transit time through this length of fiber is less than 150 ps, providing adequate time resolution for the 30-ns-wide pulse from the Febetron. After each shot, the fiber was advanced to expose a pristine section of fiber. The Febetron was typically charged to 28 kV, delivering approximately 300 kRad with no attenuation of the beam. To reduce the dose, foils of aluminum were placed between the Febetron tube and the fiber. Dose was measured using radiachromic film from Far West Technology on each shot, and typical changes in optical density ranged from 0.01 to 0.15, measured with a resolution of 0.001.

For the LINAC experiments, in order to deliver a measurable dose to the minimum length of fiber, we secured the fiber directly to the output port of the accelerator. We estimate the exposure length to be approximately 1 cm, measured by the extent of discoloration of the fiber jacket after many doses at 60 Hz repetition rate. From this length, we expect a transit time through the affected fiber to be approximately 50 ps—comparable with the nominal pulse duration of the accelerator. Even though the pulses were repeated at 60 Hz for a considerable time, the DC component of the darkening was negligible on this short length of exposed fiber.

B. Results: Sensitivity to 30 ns Pulses

The time-domain response of the Corning SMF28e to the electron pulse is shown in Fig. 3 for both amplitude (in dB) and phase (in radians). Overlaid with these traces is the time-integrated beam current, measured on several separate shots using a fast Faraday cup detector. On the time scale measured here, both attenuation and phase shift appear to integrate the dose, but the recovery of the attenuation begins promptly when the dose ends. The phase shift recovers more slowly. These results are corroborated on very short time scales by the time-domain data from the LINAC outlined below.

For comparison, the time-domain response of the phase shift for all three fibers is shown in Fig. 4. The dose is integrated by each fiber, with a slow recovery on the time scale of the delay interferometer. We speculate that the difference between the traces may be due to the acoustic effects of the different fiber constructions, which in turn produce different signatures of ultrasonic ringing. Since the onset of this effect is beyond the time scale of interest for the diagnostics in question, we will not investigate its origin in this work. We will note, though, that sub-microsecond ringing was observed in work by Girard *et al.* [10], and by Henschel *et al*. [11].

The peak attenuation and phase shift values from numerous Febetron shots are plotted versus dose in Figs. 5 and. 6. The darkening, or radiation-induced absorption, is shown in dB in Fig. 5, while the phase shift is shown in Fig. 6. The darkening of approximately 0.2 dB/m/kRad for SMF28e and for the radiation-hardened fiber compares very well with that measured using X-ray pulses on germanosilicate fibers [10]. The slopes of the least-squares linear fit to the plots in Figs. 5 and 6 are tabulated in Table I. The attenuation slopes of the three fibers are quite comparable, but the phase sensitivity of the photonic crystal fiber is appreciably lower than the SMF28e and the radiation-hardened SMF.

C. Results: Time-domain Response to 50 ps Pulses

The time-domain response of the radiation-induced attenuation and the radiation-induced phase shift appears to be instantaneous on the 50 ps time scale. The instantaneous response for both absorption and phase shifting is important for efforts to model signal degradation during intense, pulsed-radiation fields.

The three fibers are compared for their attenuation in Fig. 7, and for their phase shift in Fig. 8. The SMF28e and the radiation-hardened SMF behave comparably in both measurements, while the PCF appears to have a more pronounced, prompt recovery component.

D. Implications for System Design

The sensitivity and time response of the three fibers tested help guide the selection of transmission fibers for high-bandwidth analog data links in next-generation pulsed-power facilities. Photonic crystal fibers appear to be good choices for signal transmission, but the high cost may limit their application to short runs in the most extreme radiation environments.

For longer runs, SMF28e and the radiation-hardened fiber have similar single-shot performance. Since the cost of the fiber for each of these is low compared to the cost of cabling the fiber, the radiation-hardened fiber may be the preferred choice for permanent installation. It is not clear, however, how quickly the low shot repetition rate (less than 3 shots per day) will cause significant permanent damage to either of these fibers.

An important data set that does not yet exist is the characterization for the short-time response of new air-guiding photonic crystal fibers. Preliminary data in [10, 11] at lower doses and over microsecond time scales show promise for use of these expensive specialty fibers for short runs from the target chamber to the first barrier wall. An extra advantage would be if the effective index of refraction for the air-guiding fibers is significantly lower than the index of solid-core fibers, since the signal would propagate out of the radiation areas sooner, before the slower neutron radiation leaves the target

chamber.

IV. System Design and Data from the Omega Laser

A. M-Z System Design

We have designed and fielded an M-Z link for environments with high electromagnetic pulses (EMP) and fielded it as part of the gamma reaction history measurement at the OMEGA laser facility, supported by Los Alamos National Laboratory. The bandwidth requirements are driven by the selection of the photomultiplier tube (PMT) required to measure the Cherenkov light on the Los Alamos GCD at OMEGA. The PMT used for these experiments has a full-width-half-maximum response of approximately 80 ps, or an equivalent Gaussian bandwidth of almost 4 GHz.

Preliminary experiments at OMEGA showed that, outside the target chamber, no evidence of fiber darkening was detectable, but the high EMP entered the M-Z package and corrupted the signal. Design, then, focused on shielding the EMP from the M-Z, and the following challenges were identified:

1) High EMP in the target bay; M-Z package not RF-tight: The solution is to enclose the entire M-Z package in an RF-tight enclosure. We selected a 60 db enclosure that fit the modulator, fibers, bias network, and RF signal cable. The penetrations into the enclosure are two SMA electrical feedthroughs, and a waveguide feedthrough for the fibers.

2) Space constraints at the outside of the target chamber: To minimize the length of RF cabling, we designed the M-Z enclosure to operate as close as possible to the outside of the target chamber. This requirement drove the decision to have the modulator remote from the diode laser and the bias controller, connected by an umbilical cable with two fibers and a bias supply cable.

3) Need to supply bias voltage without picking up EMP: To prevent the DC bias line from picking up EMP, we terminate both ends of the line in 50 Ohms using commercially available bias tees. The DC port of the tee is used to supply and receive the bias voltage, while the RF port is terminated. The RF+DC port is connected to a solid-shielded coaxial cable supplying the bias. The bias supply is shown schematically in Fig. 9.

4) Need to run fibers in and out of the enclosure: We built a cylindrical waveguide feedthrough for the optical fibers, with a diameter of 0.5 in. and a length of 5 in. The inner diameter was large enough to fit both FC fiber connectors.

B. Experimental Conditions at the OMEGA Laser

Data were collected with the system described above during a high-yield deuterium-tritium fusion campaign at OMEGA on October 4, 2006 [12]. Laser energies for the high-yield shots that day were between 26.8 and 28.2 kJ in 60 beams. The yields ranged from 8.3×10^{13} to 8.8×10^{13} neutrons. The data presented below were for shot number 45048, with a pulse-energy of 28.2 kJ and a yield of 8.78×10^{13} neutrons.

The data were collected on a single channel of a 12 GHz digitizer at 40 GS/s, using a DC-coupled photoreceiver with an inverting preamplifier.

C. Data and Analysis

The samples from the digitizer are shown as open circles in Fig. 10. The modulator was initially biased at its quadrature point (50% transmission), and the light level goes toward zero as the signal arrives from the PMT, going through a modulation extremum at 3.3 ns before the input voltage peaks at 3.35 ns and returns to zero, causing the modulator to go back through the modulation extremum at 3.4 ns.

The curves shown in Fig. 10 are the first ten Monte Carlo simulations of signals where we have used the RMS noise value before the shot to compute possible voltage values at each sampling time. The simulated points are then interpolated using sin(x)/x interpolation to improve the estimate of the recorded voltage at the modulation extrema. In addition to randomization of the digitizer record itself, we also randomized for each trial the unfold parameters, φ_0 and V_{Max}, with V_{Min} implicitly randomized by calculation from the simulated digitizer record.

We generated one hundred Monte Carlo simulations of this sort, and for each one we calculated the appropriate envelope and unfolded the data using the arcsine function described in (2). Statistics were then calculated on the one hundred simulated records to compute a 95% confidence band for the unfolded data.

The unfolded digitizer points and the 95% confidence band are shown in Fig. 11. The upper half of the peak has measurably larger error bands because of the sensitivity of the unfolded data to noise near the modulation extrema. This loss of sensitivity highlights a design requirement for systems where the expected signal level may not be well known; two approaches to covering such an experiment are (a) two or more M-Zs, or (b) a phase modulator demodulated with non-complementary outputs.

The Monte Carlo simulations give insight into the contribution of the noise to the uncertainty in the processed data. Such error bars are routinely requested by computational physicists when modeling the hydrodynamics of nuclear interactions, so we are continuing with efforts to cover greater dynamic range and implement more sophisticated data analysis techniques. With overlapping records from multiple M-Zs on multiple scope channels, we expect to more fully exploit least-squares fitting [6].

V. Conclusion

We have considered the sources of error in the high-bandwidth analog fiber-optic links that are expected to play an increasingly vital role in inertial-confinement fusion experiments. The sinusoidal transfer function of interferometric links is deterministic, and it allows us to include known calibration uncertainties in the data analysis to compute rigorously-defined error bars. Radiation effects on the fibers have different magnitudes for amplitude and phase, though in each case, the net effect is to increase the

uncertainty in the final data. Careful system design is the key to engineering a robust fiber link that can accommodate the next generation of fusion experiments and high-bandwidth diagnostics.

REFERENCES

[1] E. J. Friebele, *et al.*, "Interlaboratory comparison of radiation-induced attenuation in optical fibers. Part III: Transient exposures," *J. Lightwave Technol.*, vol. 8, no. 6, pp. 977–989, June 1990.

[2] S. Girard, J. Baggio, J.-L. Leray, J.-P. Meunier, A. Boukenter, and Y. Ouerdane, "Vulnerability analysis of optical fibers for laser megajoule facility: Preliminary studies," *IEEE Trans. Nucl. Sci.* vol. 52, no. 5, pp. 1497–1503, Oct. 2005.

[3] M. J. May, *et al.*, "High bandwidth data recording systems for pulsed power and laser produced plasma experiments," *Rev. Sci. Instrum.,* vol. 77, no. 10, pp. 10F504.1–10F504.3, Oct. 2006.

[4] J. M. Mack, *et al.,* "Multiplexed gas Cherenkov detector for reaction-history measurements," *Rev. Sci. Instrum.,* vol. 77, no. 10, pp. 10E728.1-10E728.4, Oct. 2006.

[5] C. J. Horsfield, *et al,* "Gamma-ray bang-time measurements with a gas Cherenkov detector for interial-confinement fusion experiments," *Rev. Sci. Instrum.,* vol. 77, no. 10, pp 10E724.1–10E724.3, Oct. 2006.

[6] J. J. Blair, "Error estimates derived from the data for least-squares spline fitting," presented at the 2007 Int. Conf. on Measurement Technology, Warsaw, Poland.

[7] C. A. de Boor, *A Practical Guide to Splines – Revised Edition*. New York, NY: Springer-Verlag, 2001.

[8] E. W. Taylor, *et al.*, "Interlaboratory comparison of radiation-induced attenuation in optical fibers. Part II: Steady-state exposures," *J. Lightwave Technol.*, vol. 8, no. 6, pp. 967–976, June 1990.

[9] S. Girard, *et al.*, "Pulsed x-ray and gamma-ray irradiation effects on polarization-maintaining optical fibers," *IEEE Trans. Nucl. Sci.,* vol. 51, no. 5, part 3, pp. 2740–2746, Oct. 2004.

[10] S. Girard, J. Baggio, and J.-L. Leray, "Radiation-induced effects in a new class of optical waveguides: the air-guiding photonic crystal fibers," *IEEE Trans. Nucl. Sci.,* vol. 52, no. 6, part 1, pp. 2683–2688, Dec. 2005.

[11] H. Henschel, J. Kuhnhenn and U. Weinand, "High radiation harndess of a hollow core photonic bandgap fiber," presented at RADECS 2005, Cap d'Agde, France.

[12] H. Herrmann, et al, "Improved gamma bang-time measurements on Omega and implications for the National Ignition Facility," Journal of Physics: *Conference Series,* submitted for publication.

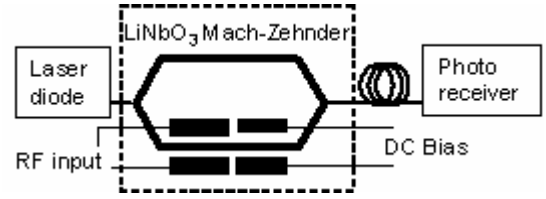

Fig. 1. Schematic diagram of M-Z amplitude-modulated fiber-optic link. The dashed line encloses the modulator, which is typically 10 cm long. Fibers can be arbitrarily long in general, but the fiber from the source laser is polarization-maintaining and should ideally be kept to 5 m length, or less.

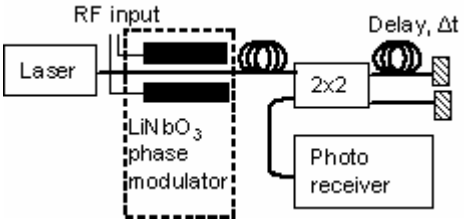

Fig. 2. Schematic diagram of a phase-modulated fiber-optic link. The dashed line encloses the modulator, which is typically in a package very similar to the M-Z package. For Δt less than a few nanoseconds (differentiation on long pulses, direct signal measurement on very short pulses), a diode laser may be used; for Δt greater than a few nanoseconds, a long-coherence-length laser such as a fiber laser should be used. The demodulation interferometer shown is the simplest configuration, using Michelson geometry.

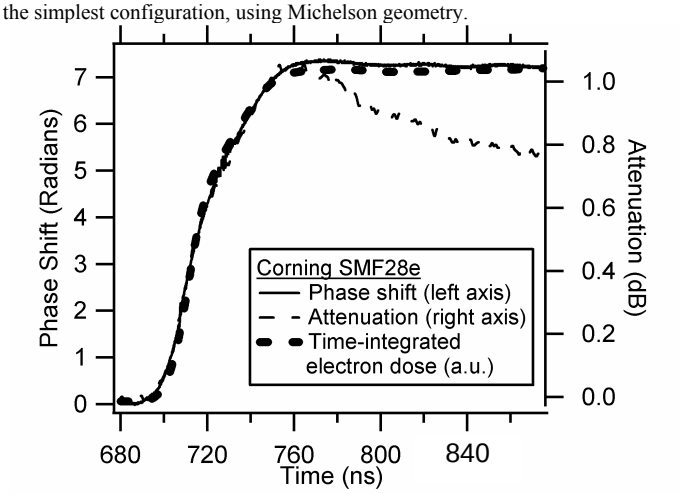

Fig. 3. Phase shift and attenuation of Corning SMF28e fiber during and immediately after exposure to the 30 ns pulse from the Febetron 705. Total dose for this shot was 238.5 kRad.

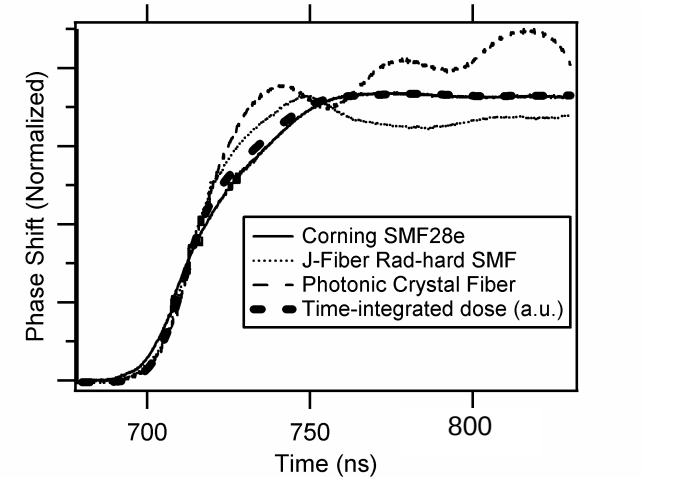

Fig. 4. Time response of the phase shift to a 30 ns wide electron pulse from the Febetron 705. The phase generally integrates the dose during exposure and recovers slowly for all three fibers tested.

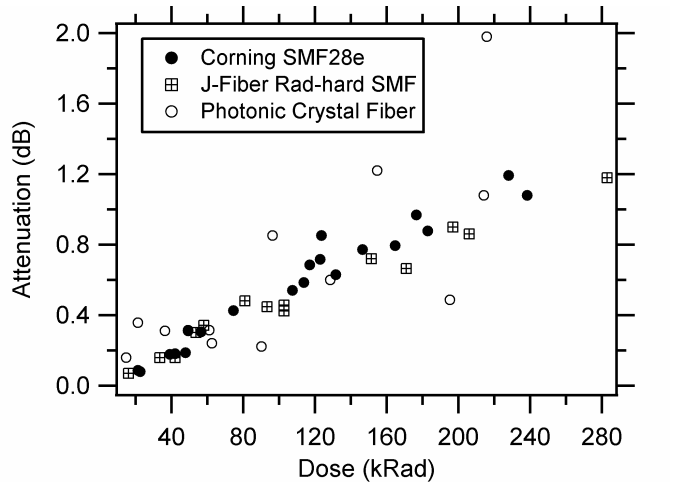

Fig. 5. Attenuation versus dose in the Febetron experiment for the three fibers tested using 2.5 cm exposure length.

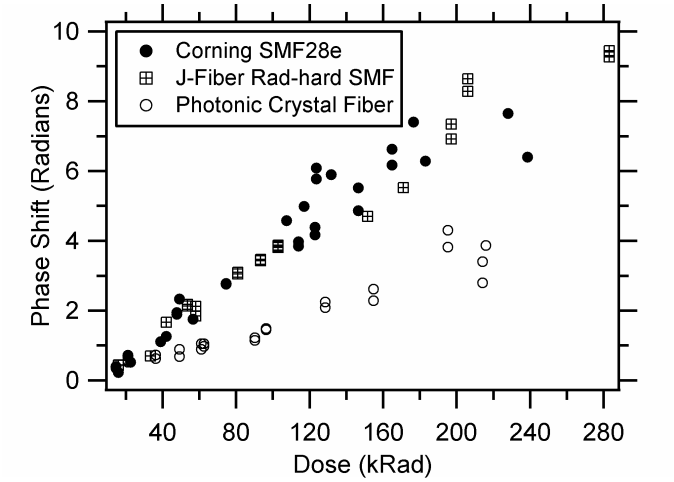

Fig. 6. Phase shift versus dose in the Febetron experiment for the three fibers tested using 2.5 cm exposure length.

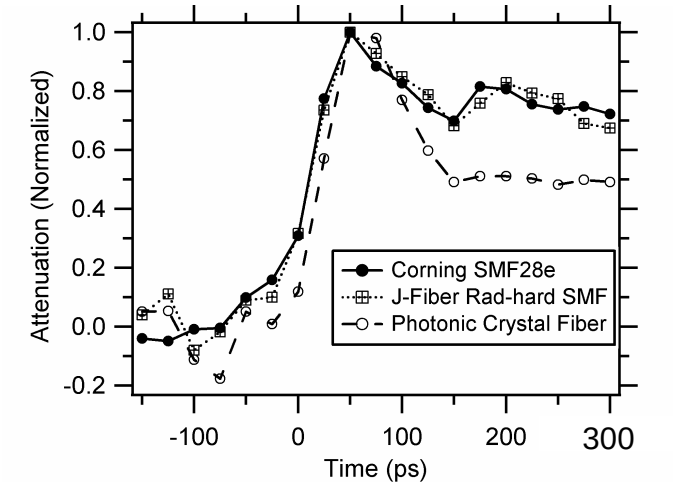

Fig. 7. Time response of the induced attenuation in the LINAC experiment for the three fibers tested using approximately 1 cm exposure length.

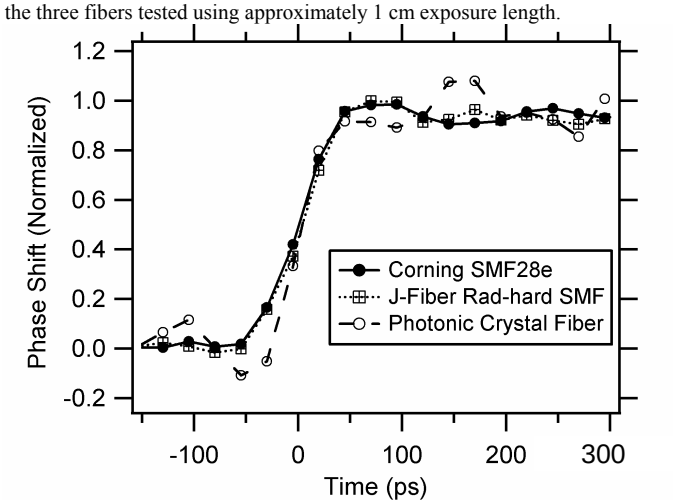

Fig. 8. Time response of the induced phase shift in the LINAC experiment for the three fibers tested using approximately 1 cm exposure length.

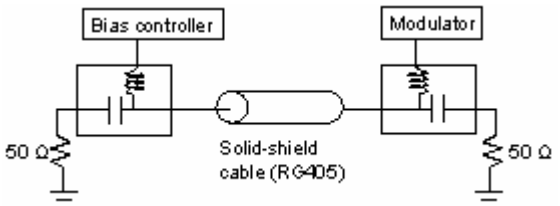

Fig. 9. Schematic of M-Z bias supply line, showing implementation of bias networks to terminate high frequencies in 50 Ohms.

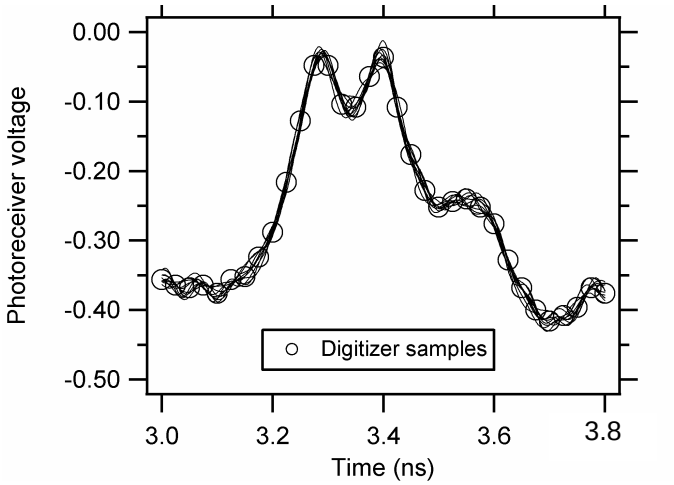

Fig. 10. Raw digitizer data (open circles) from the OMEGA experiment, together with ten of the one hundred Monte Carlo–simulated records used in the error estimation.

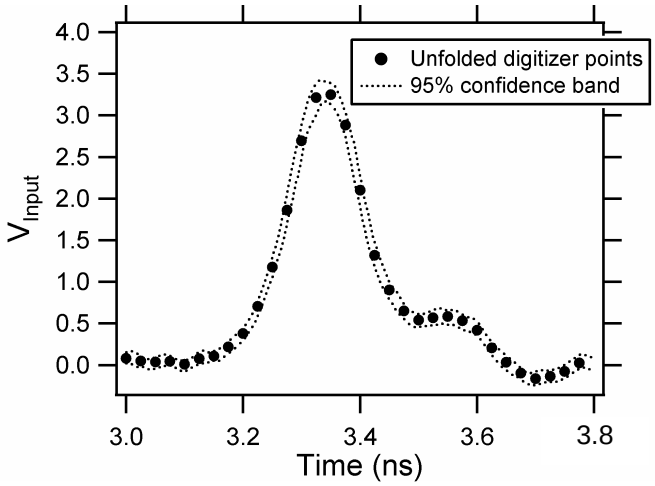

Fig. 11. Unfolded digitizer data (circles) from the OMEGA experiment, together with the 95% confidence bands from the Monte Carlo simulations.

TABLE I
SENSITIVITY OF FIBERS TO RADIATION PULSES

Fiber	Phase (Radians/kRad/m)	Attenuation (dB/kRad/m)
Corning SMF28e	1.54	0.21
J-Fiber Radiation-hardened SMF	1.45	0.18
Photonic Crystal Fiber	0.67	0.23